Current Applied Physics 10 (2010) 428–435

Contents lists available at ScienceDirect

Current Applied Physics

journal homepage: www.elsevier.com/locate/cap

Characteristics of nitrogen-incorporated silicon oxycarbide films and plasmas for plasma enhanced chemical vapor deposition with TMOS/N_2/NH_3

C.J. Chung, T.H. Chung *, Y.M. Shin, Y. Kim

Department of Physics, Dong-A University, 840 Hada-dong, Saha-Gu, Busan 604-714, Republic of Korea

ARTICLE INFO

Article history:
Received 4 July 2008
Received in revised form 12 May 2009
Accepted 26 June 2009
Available online 7 July 2009

PACS:
52.75.Rx
52.25−b
73.90+f

Keywords:
Nitrogen-incorporated silicon oxycarbide thin film
Tetramethoxysilane
Plasma enhanced chemical vapor deposition

ABSTRACT

Plasma enhanced chemical vapor deposition of nitrogen-incorporated silicon oxycarbide thin films obtained from the gas mixture of TMOS (tetramethoxysilane), N_2, and NH_3 is studied. The effects of the TMOS to N_2 pressure ratio on the properties of the film and the plasma are investigated. The deposited films are analyzed by in situ ellipsometry, ex situ Fourier transform infrared spectroscopy (FTIR), and by X-ray photoelectron spectroscopy (XPS). The plasma is characterized by using optical emission spectroscopy (OES). The mass spectra of the constituents in the plasma are obtained by quadrupole mass spectroscopy. The correlation between the film properties and the plasma characteristics is explained wherever possible. As the partial pressure of N_2 is decreased, the refractive index begins to decrease, reaches a minimum, and then saturates. The FTIR absorption bands are observed from about 850 to 1000 cm^{-1} and from 1000 to 1250 cm^{-1}, and can be attributed to the formation of a nitrogen-incorporated silicon oxycarbide thin film. The variation of the refractive index is discussed in relationship with the deposition rate, the OES spectra, the mass spectra of the plasma, the film composition obtained by XPS, and FTIR spectra.

© 2009 Elsevier B.V. All rights reserved.

1. Introduction

Nitrogen-incorporated silicon oxide thin films are being widely used not only as masking and passivation layers in microelectronic circuits but also in optical filter fabrication because of their excellent properties such as continuously variable refractive index [1–3]. The refractive index can be changed from pure silicon dioxide to silicon nitride by just varying the film composition. Nitrogen-incorporated silicon oxide thin films can be formed either by high-temperature or low-temperature techniques. Plasma enhanced chemical vapor deposition (PECVD), remote PECVD, and low-pressure CVD are typical low-temperature processes while rapid thermal processes and nitridation of SiO_2 films in NH_3 or N_2 atmospheres are typical high-temperature processes. Although a high control of deposition parameters is not adequate, plasma enhanced chemical vapor deposition has been one of the most important thin film processes because of the possibility of preparing good quality coatings at low substrate temperature [4].

In previous works [5,6], nitrogen-incorporated silicon oxide thin films were deposited from plasma enhanced chemical vapor deposition with TMOS (tetramethoxysilane: $Si(OCH_3)_4$) and N_2O as precursor gases. An incorporation of nitrogen was observed by Fourier transform infrared spectroscopy (FTIR) and X-ray photoelectron spectroscopy (XPS). However, the nitrogen content was small and the refractive index was less than 1.55. In this study, nitrogen-incorporated silicon oxycarbide thin films ($SiO_xC_yN_z$) are prepared with the purpose of optical applications in a PECVD reactor by using TMOS, NH_3, and N_2 as precursor gases.

One of major concerns in PECVD techniques is the lack of knowledge of the processes that are taking place and the species in the plasma that may be involved in the deposition process. Using experimental techniques such as plasma mass spectrometry or optical emission spectroscopy, it is possible to gain insight about the species and the processes in the plasma [7]. In this work, the PECVD plasma is characterized using optical emission spectroscopy (OES) and the behavior of gaseous species in the plasma is measured by mass spectroscopy. The optical properties of the deposited films are characterized by refractive index measurements using in situ ellipsometry. The characterization of the deposited film is also performed by ex situ Fourier transform infrared spectroscopy and by X-ray photoelectron spectroscopy.

The correlation between the properties of the deposited films and the plasma characteristics is explained to some extent. Specifically, one of the aims of this paper is to study the effects of the partial pressure ratio of TMOS to N_2 in the gas (while maintaining a constant chamber pressure with a fixed partial pressure of NH_3 as 5% and a fixed RF input power) on the optical properties of

* Corresponding author.
E-mail address: thchung@dau.ac.kr (T.H. Chung).

1567-1739/$ - see front matter © 2009 Elsevier B.V. All rights reserved.
doi:10.1016/j.cap.2009.06.056

the deposited film. The inclusion of NH_3 facilitates the surface interaction [8] and has been found to enhance the incorporation of nitrogen in the deposited films [9]. The properties of the deposited thin films are determined by changing the relative flows of precursor and nitrogen. As a typical example of the film property, the variation of the refractive index is discussed in relationship with the deposition rate, the OES spectra, the mass spectra of the plasma, the film composition obtained by XPS, and FTIR spectra.

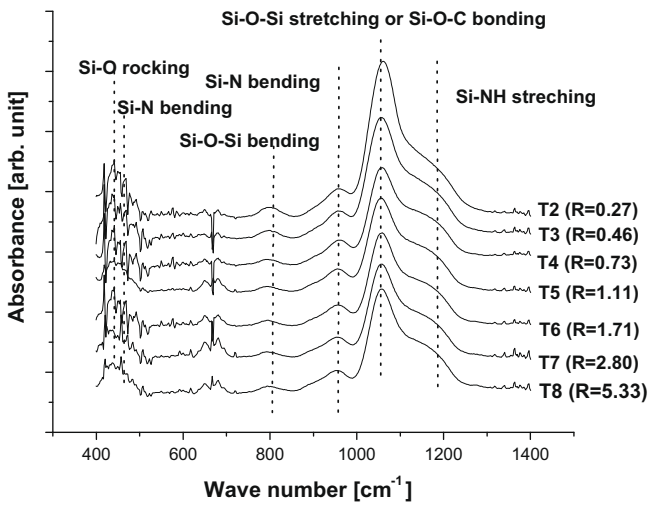

Fig. 1. FTIR spectra for films deposited at various partial pressure ratios, where $P = 500$ W and $p = 10$ mTorr.

2. Experiment

The PECVD reactor utilizes an inductively coupled plasma source operating at 13.56 MHz to sustain low-pressure (1–50 mTorr) high-density plasmas. The inductively coupled plasma yields a high degree of ionization and significant decomposition of the precursor. Nitrogen and NH_3 are used as the reactant gas for production of plasma, and TMOS is used as volatile precursor of silicon. The gas flows of TMOS, N_2, and NH_3, regulated by mass flow controllers (AFC 50), are introduced downstream from the plasma about 10 cm above the substrate. Further details of the plasma source have been described in the previous studies [5,6]. The films are deposited on p-type Si(1 0 0) substrates at room temperature.

The partial pressure of the organosilicon compound and that of nitrogen gas are controlled by mass flow controllers. The parameter R is defined as the ratio of partial pressure of the TMOS gas to the N_2 gas (i.e., $R = p(\mathrm{TMOS})/p(\mathrm{N_2})$) and then the total pressure is fixed at 10 mTorr. Deposition studies are carried out as functions of the radio frequency power and the N_2 fraction (R). The samples are numbered from T1 (p(TMOS): p (N_2) = 0.1: 0.85) to T8 (p(TMOS): p (N_2) = 0.8: 0.15). The thickness and refractive index are measured by using in situ ellipsometer (Elli-situ 2000, Ellipso Tech) operating at the He–Ne laser wavelength (632.8 nm).

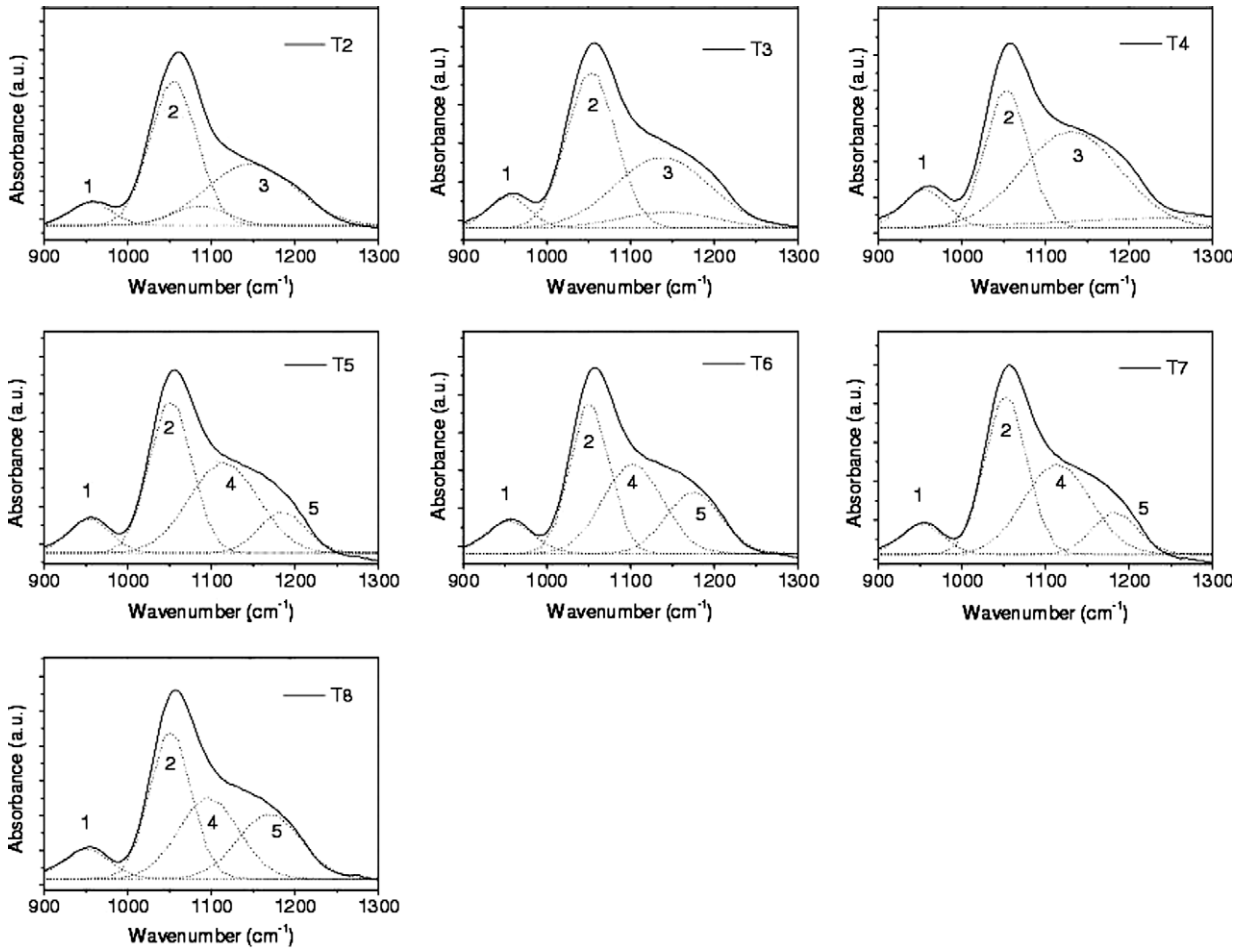

Fig. 2. Deconvolution of the broad peak in the wavenumber range from 1000 to 1300 cm^{-1} of the FTIR spectra for the thin films T2–T8.

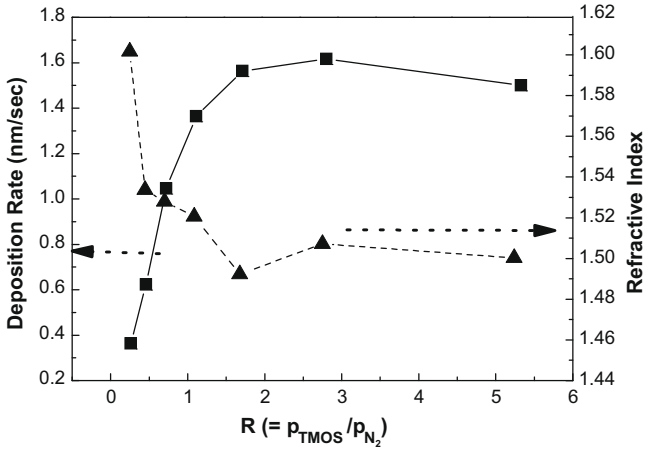

Fig. 3. Deposition rate and index of refraction as functions of the partial pressure ratios of TMOS and N_2, *R*, where $P = 500$ W and $p = 10$ mTorr.

The deposition rate is determined from the ratio of the film thickness to the deposition time. The chemical bonding states of the deposited films are analyzed by a Fourier transform infrared spectrometer (BIO RAD Excalibur). The chemical structure and the composition of the films are estimated by using an X-ray photoelectron spectroscopy (ESCA/Auger system). The light intensities of emissive molecules and radicals in the plasma are collected by an optical fiber that is coupled to multi-channel spectrometer (OPC-2000). Emission light from glow discharge is detected through an optical probe during deposition in the wavelength range of 400–900 nm with a resolution of 1 nm. The dependence of the emission intensities on the process parameters is investigated.

In these experiments, a quadrupole mass spectrometer (Pfeiffer Vacuum, QMS 200F2) is mounted to the main chamber. A 100 micrometer-diameter aperture connects the QMS analysis section with the main chamber. The gas collected through the orifice is ionized and analyzed by the spectrometer. The distinction between ions and neutral species formed in plasma is not made in this experiment. Experimental mass spectra are recorded in the mass range 1–200 amu with a resolution of 0.5 amu. The mass spectrometer system is evacuated by a turbo molecular pump (TMU071P) backed by a rotary pump (DUO 2.5). The residual pressure in the mass spectrometer is 10^{-7} Torr and the pressure increases up to 10^{-5} Torr during the experiments.

3. Results

3.1. Characterization of deposits

Fig. 1 shows FTIR spectra of films deposited at various values of *R*. The ICP power is fixed at 500 W. The spectra are obtained from films with the same thickness (200 nm). The spectra exhibit absorption peaks at 1045–1075 cm^{-1} corresponding to Si–O–Si stretching band, at 810 cm^{-1} corresponding to Si–O–Si bending, at 460 cm^{-1} corresponding to Si–O–Si rocking mode. The broad peak at 1000–1250 cm^{-1} corresponds not only to Si–O–Si, but also Si–O–C and even Si–C–Si [10]. The peak around 960 cm^{-1} is most probably related to the stretching vibrational mode of Si–N–Si bonds, which is evidence that nitrogen incorporates in the oxide

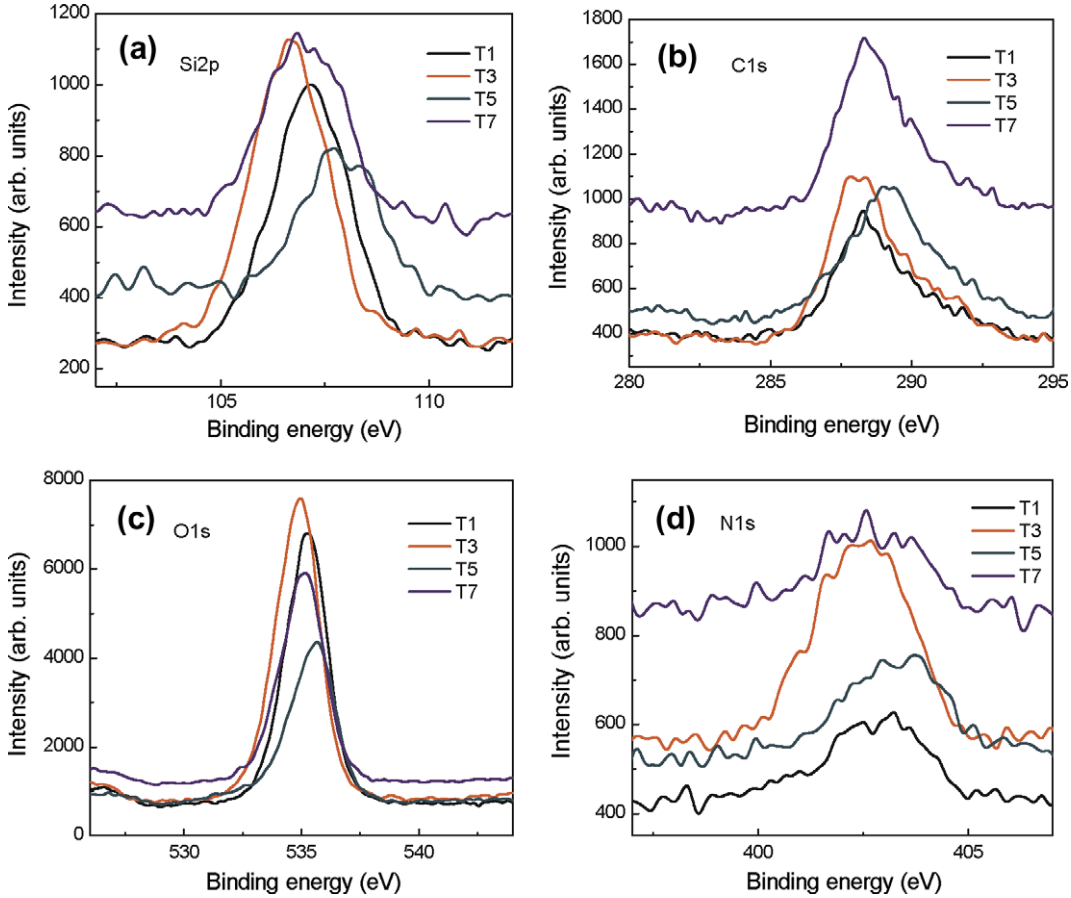

Fig. 4. XPS narrow scan spectra (a) Si 2p, (b) C 1s, (c) O 1s, and (d) N 1s of the nitrogen-incorporated silicon oxycarbide thin films obtained from TMOS/N_2/NH_3.

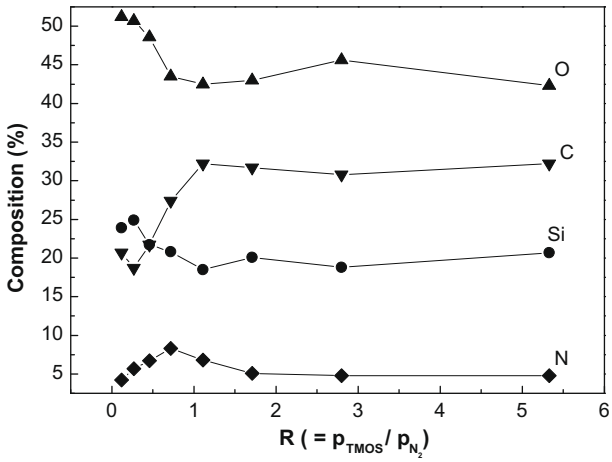

Fig. 5. Variation of the atomic concentration of the elements in the deposited film as a function of *R*.

network [11,12]. However, it is overlapped by the rocking mode for Si–CH_3. In addition, a weak and shallow band appears within 1120–1180 cm^{-1} which can be attributed to the bending vibration of N–H bonds in the oxynitride network [12]. Since the nitrogen content in the film is only few percent, the 960 cm^{-1} Si–N peak appears as a shoulder of a strong Si–O–Si stretching mode. The absorption bands observed from 850 to 1000 cm^{-1} and from 1000 to 1250 cm^{-1}, which can be attributed to the formation of a nitrogen-incorporated oxycarbide, become dominant as the *R* increases. As the nitrogen content is increased, the absorption bands are broadened and shifted to lower wave numbers [13,14]. The shifts can be attributed to an increase of the nitrogen atom density in the silicon tetrahedral environments [15]. In addition, there are also SiNH bending mode and silicon atom breathing modes evident at 1175 and 475 cm^{-1}, respectively [14,16]. The absorption peaks at 900 and 1263 cm^{-1} corresponding to Si–OH and $SiCH_3$, originating from the hydrocarbons from incompletely dissociated TMOS, are not observed.

The broad peak at 900–1300 cm^{-1} is deconvoluted for the samples T2–T8 by using the Gaussian peak fitting in Fig. 2. The four or five fitted peaks are attributed to the Si–O–Si stretching mode (or Si–O–C bonding mode) at 1065 cm^{-1} (curve 1), the stretching mode of Si–N–Si bonds at 960 cm^{-1} (curve 2), cage linked Si–O–C bonding mode at 1090–1100 cm^{-1} (curve 4), Si–C bonding mode (or larger angle Si–O–Si bonds in a cage structure [17]) at 1140 cm^{-1} (curve 3), and cage linked Si–C bonding mode at 1180 cm^{-1} (curve 5). The Si–O–Si stretching band frequency shifts are attributed to changes in the Si–O–Si bonding angle. In fully relaxed stoichiometric thermal silicon oxides, the bonding angle is reported to be ~144° with a FTIR absorption around 1080 cm^{-1}. However, in PECVD silicon oxides, the FTIR stretching frequency has been shown to decrease from 1080 to 1060 cm^{-1} as the Si–O–Si bonding angle decreases [17]. However, the broadening of the Si–O–Si stretching mode remains almost unchanged in the samples T2 through T8. It is also observed that for a high *R* region

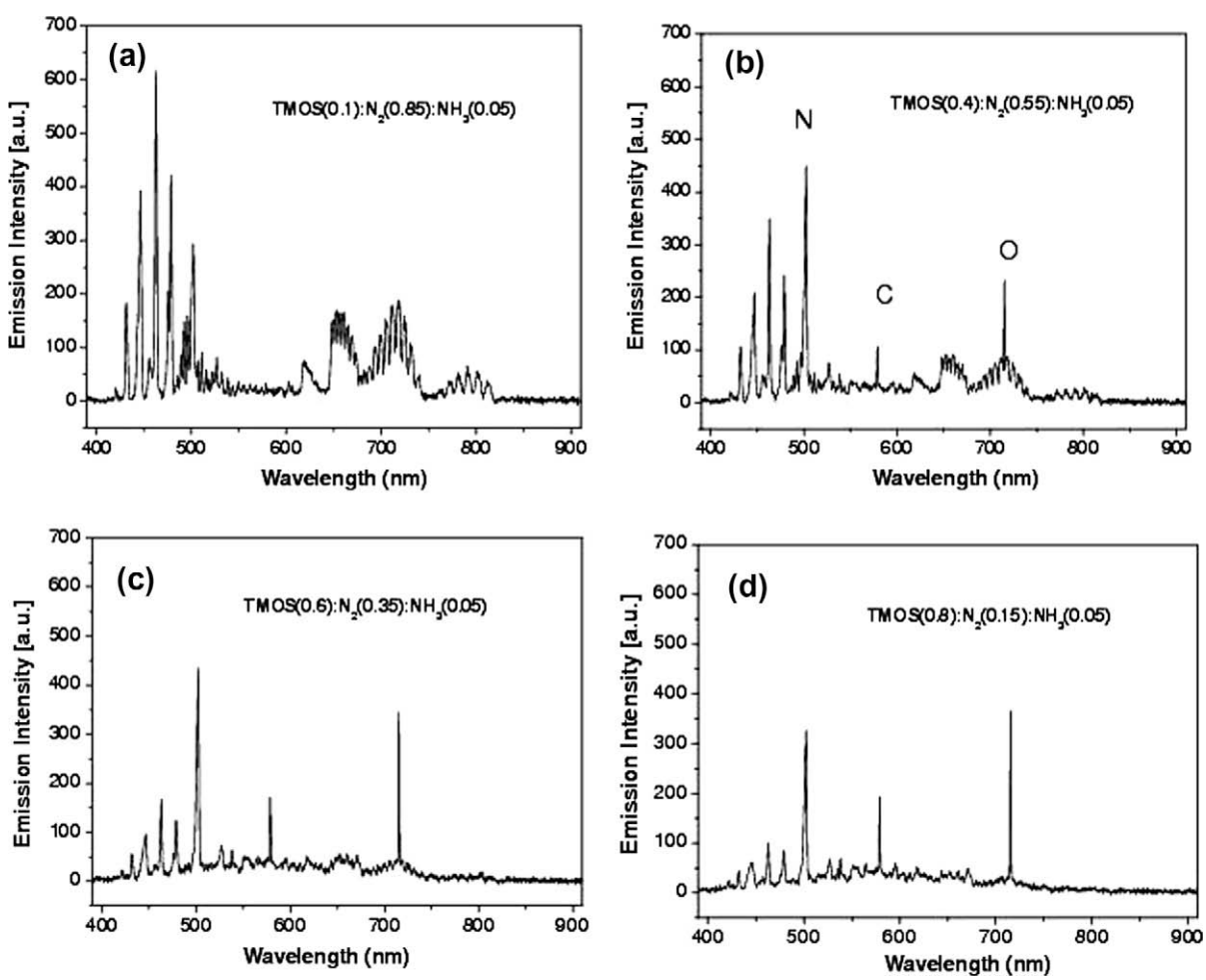

Fig. 6. Optical emission spectrum of TMOS/N_2/NH_3 plasma for various TMOS and N_2 pressure ratios where $P = 500$ W and $p = 10$ mTorr.

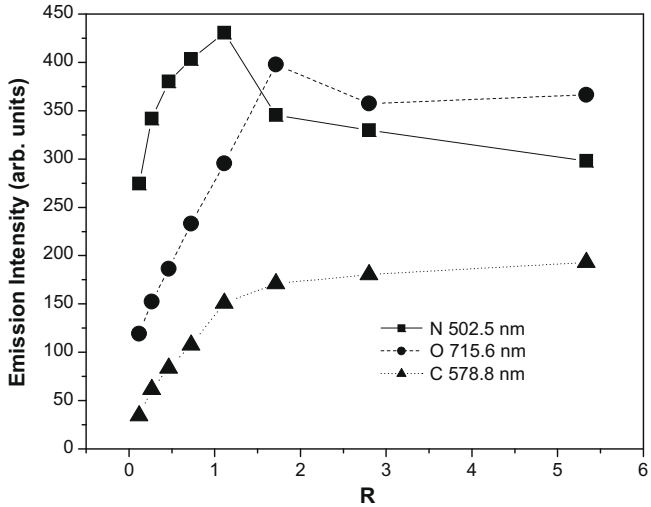

Fig. 7. Evolution of the intensities of the selected oxygen, carbon, and nitrogen emission lines with the pressure ratios of TMOS and N_2.

(T4–T8), the cage linked Si–C bonding mode at 1180 cm^{-1} becomes dominant. All samples have a similar shape of the peak at 960 cm^{-1} indicating the Si–N–Si bonds. The T2 film has the small peak of the Si–N–Si bonds while the T4 film has the largest peak.

Fig. 3 shows the variation of the deposition rate and the refractive index as a function of *R*. The ICP power and the total pressure are kept constant at 500 W and 10 mTorr, respectively. It is observed that the increase in the TMOS partial pressure causes an increase in the deposition rate. This could be accounted for from an increase in the frequency of the electron impact dissociation of the precursor as *R* increases. As can be seen, the refractive index lies between 1.43 and 1.60. These values are little higher than that of thermal SiO_2 ($n = 1.45$). However, these values are quite low compared to those of other SiON (between 1.6 and 1.9) [18]. As *R* increases, the refractive index tends to decrease. We attribute the decrease in the refractive index to the incorporation of oxygen and carbon atoms [19]. We can attribute the increase in the refractive index to an incorporation of more nitrogen atoms. These assumptions should be examined by OES and XPS data.

Above predictions are confirmed with X-ray photoelectron spectroscopy. The XPS narrow scan spectra for several samples are shown in Fig. 4. Supposing the quantity of surface charging is about 3 eV, the peak positions of the Si 2p, O 1s, C 1s, and N 1s for the T3 sample are located at binding energies of 103.7 eV, 531.9 eV, 284.8 eV, and 399.6 eV, respectively. The films exhibit a weak N 1s peak, but its intensity is below the detection limit of XPS analyses, precluding a quantitative analysis of the nitrogen content in the films. The reported peak positions of the Si 2p, O 1s, and C 1s for silicon oxide obtained from TMOS/O_2 were 103.5 eV, 532.9 eV, and 284.8 eV, respectively [20,21]. The results show that the position and the full width at half maximum values

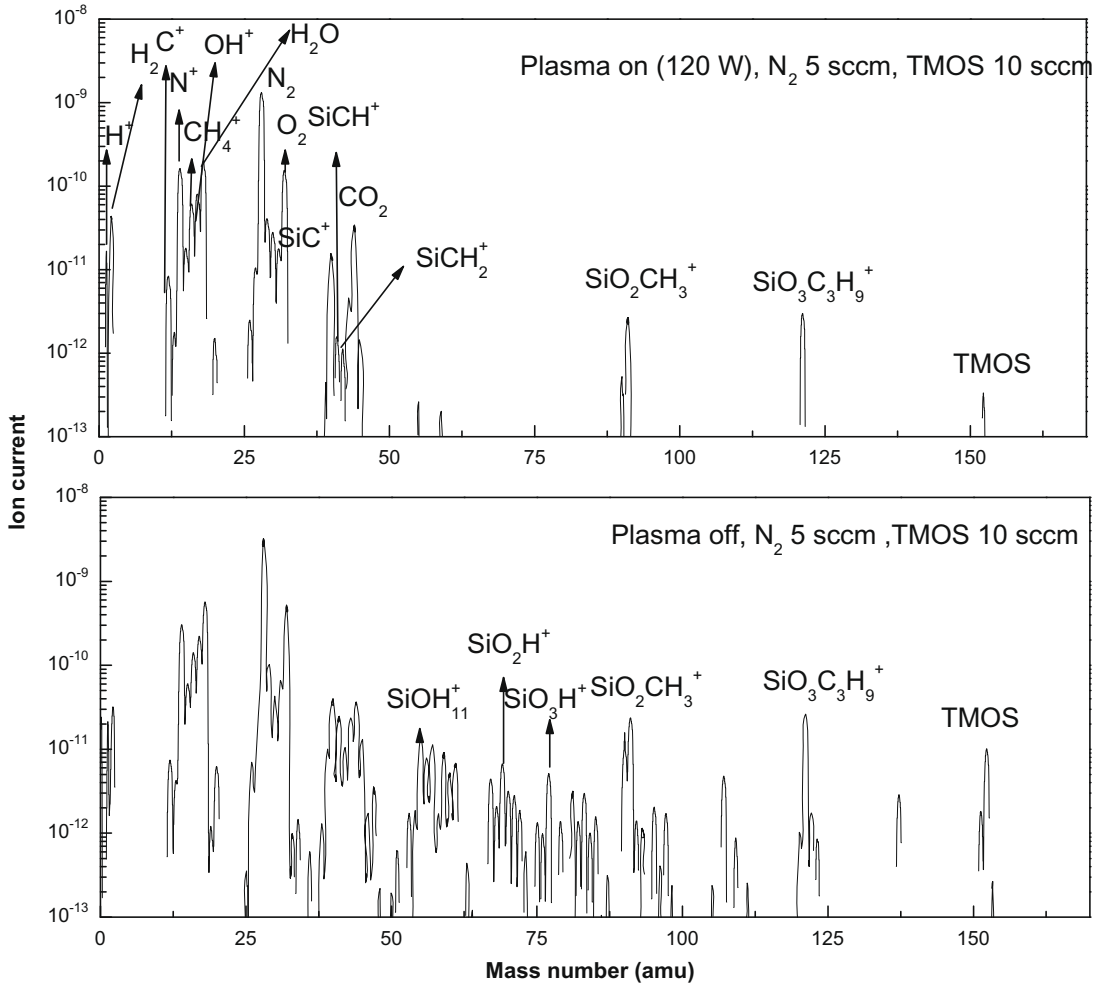

Fig. 8. Mass spectra of TMOS and N_2 gas mixture with plasma discharge on and off.

of the peaks change with the nature and composition of the deposit. By increasing TMOS fraction, the Si 2p spectrum is not symmetrical due to the presence of Si–O, Si–C and Si–H bonds, as shown in Fig. 4a. The peak position of C 1s has range from 284 to 286 eV depending on the parameter condition of this study. The carbon peak has higher binding energy than the results of other PECVD SiOCH films showing three different modes such as $C–O_1$ (284.18 eV), $C–O_2$ (285.88 eV) and $Si–CH_3$ (282.56 eV) [22]. The C 1s spectrum also has an asymmetric shape due to degrading at higher binding energy. The Si–C and C–O bonds are supposed to raise C 1s tail [21]. Thus it may be stated that the inclusion of N atoms modifies the chemical structure compared to the typical silicon oxide films. The N 1s peak position has range from 399 to 401 eV. Among the samples shown, T3 sample has the largest integrated area of the N 1s peak. The N 1s photoelectron peak confirms that nitrogen in the deposited film has different bonding states possessing higher binding energy than Si–N configuration (392.7 eV) and Si–N–O configuration (397.6 eV) [23]. This is also a little different from the reported peak positions for silicon oxynitride [24]. This suggests that the bond structure is Si_2 = N–O–Si [25].

The evolution of the composition of the films expressed as the percentage of atoms obtained from XPS measurement is shown in Fig. 5. A larger nitrogen fraction results in larger nitrogen content in films. The results show that the nitrogen content in the films increases with R up to 8.6% at the point of $R = 0.73$, then slightly decreases and saturates, whereas the oxygen content shows the opposite behavior in varying R. The films prepared from TMOS contain a large amount of carbon impurities. The carbon content first increases with the partial pressure of TMOS and then saturates, whereas the Si content shows the opposite behavior, similar to that of the oxygen content. The values of C/Si content ratios significantly differ according to the organosilicon [4]. The C/Si ratio in $TMOS/N_2/NH_3$ – derived films in this work is higher than in $TMOS/O_2$ – derived films [20,21]. The trend of variation in carbon content of the samples is in agreement of the deconvoluted FTIR peaks shown in Fig. 2. The O/Si ratio is always larger than two. The concentrations of nitrogen and carbon atoms in the films vary, respectively, in similar fashions to those in the plasma phase. However, the concentration of oxygen atoms in the films shows a different tendency from that in the plasma phase. As is noted in Fig. 3, the refractive index tends to decrease as the R increases. We attribute the decrease in the refractive index to the incorporation of oxygen and carbon atoms, and attribute the increase in the refractive index to the incorporation of more nitrogen atoms. The variation of the refractive index with R might be determined by a combinatory effect of nitrogen, oxygen, carbon, and silicon atoms. The increase in N atom content for the region of $R < 1$ is compensated by the high level of oxygen atom concentration and by the increase in the carbon atom content. That might explain the behavior of the refractive index as a function of R.

3.2. Characterization of plasmas

For a more complete understanding of the plasma deposition conditions, we have measured the optical emissions from the discharges with various $TMOS/N_2$ pressure ratios. Fig. 6 shows emis-

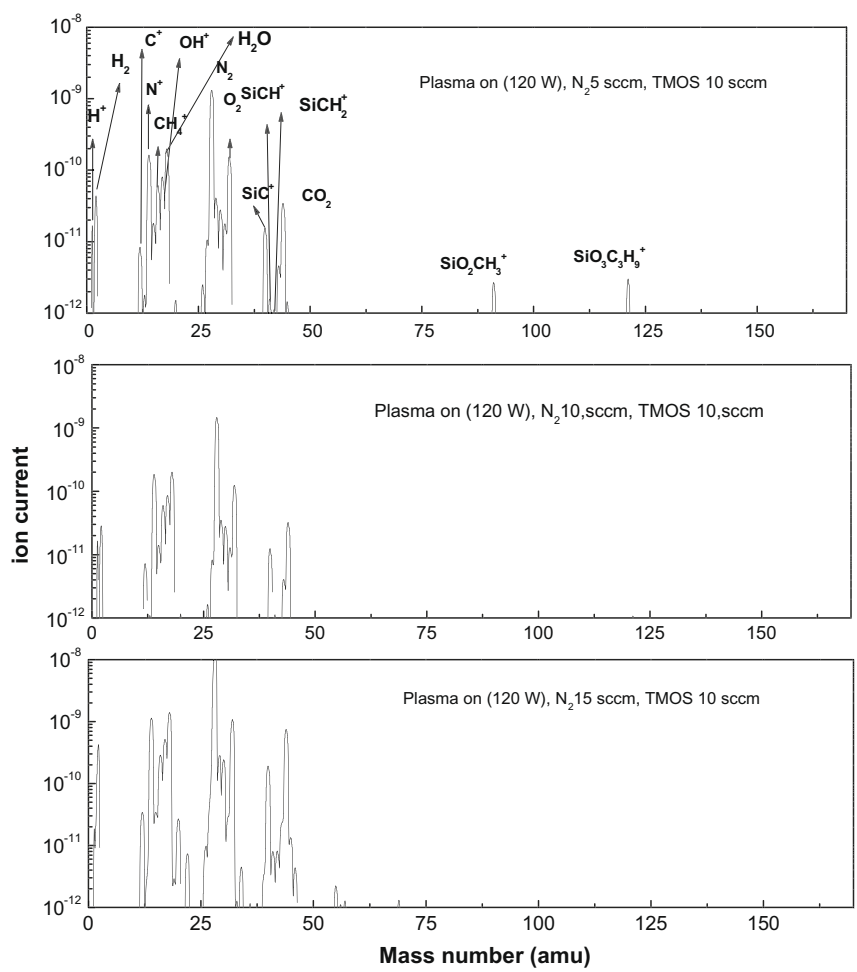

Fig. 9. Mass spectra during discharge at various N_2 flow rate for TMOS and N_2 gas mixture with total pressure of 20 mTorr.

sion spectra corresponding to four different conditions of the plasma. It is observed that for N_2 dominant discharge (a), the contribution of TMOS to OES spectrum is very weak. The OES spectrum (a) is not deviated much from that for the N_2 only case (not shown in figures). For the discharges containing a larger portions of TMOS as in (b), (c), (d), the dominant peaks are N_2 molecular peaks (the first positive system 550–800 nm), oxygen atom peak (715.6 nm), C atom peak (578.8 nm), N atom peak (502.5 nm), CH (431 nm), C_2 (516 nm), N_2^+ (479 nm). H_γ (434 nm) peaks. Especially, the strong emission features of O_I (715.6 nm), C_I (578.8 nm), and N_{II} (502.5 nm) are observed. Peaks of Balmer emission lines of atomic hydrogen, H_δ (410 nm), and the bands associated with CO, OH, C_2, and CH species coming from the fragmentation of TMOS are also present in the discharge, but the signals are weak compared to those for TMOS/O_2 discharges [26]. The emission peaks originated from N_2 gas almost disappear in (d).

The evolution of the intensity of selected oxygen, carbon, and nitrogen lines can provide some insight on the variation of the plasma properties with TMOS/N_2 pressure ratio. Fig. 7 shows the evolution of emission intensity peaks of O_I (715.6 nm), C_I (578.8 nm), and N_{II} (502.5 nm) as a function of the TMOS/N_2 pressure ratio. The emission intensity from O atom starts to increase with increasing R and reaches maximum at $R = 1.71$ where the refractive index has the lowest value. Afterwards, the intensity from oxygen atoms saturates. On the other hand the emission intensity from N atom reaches maximum at $R = 1.11$ and then decreases slightly afterward. The emission intensity from C atom continues to increase with increasing R. Since the actinometry measurement is not performed in this work, it is difficult to assume that the intensity of the emitted light is proportional to the density of ground state species. However, the excitation cross sections and the threshold values of these atoms are not quite different, and thus it may be stated that the intensity of emitted light can provide some clue on the evolution of atomic abundance in the plasma. The behavior shown in Fig. 7 suggests that oxygen and nitrogen species are formed by dissociation of the precursor and nitrogen molecule and experiences a sharp increase up to the maximum point as a function of R. The formation of activated species of both oxygen and nitrogen is effective for the $R > 1$ region. On the other hand, the carbon content increases smoothly with increasing R.

Fig. 8 shows that mass spectra of the neutral species obtained with the N_2/TMOS plasma switched off and with applying the RF power of 120 W. The ion species observed in mass spectra can result from the TMOS fragmentation in the mass spectrometer or they are ions related to neutral products formed in the plasma [27]. In order to know the origin of the species responsible for the neutral mass spectra, the mass spectra obtained with the plasma switched off is compared with those obtained when the plasma is switched on. The mass number of 1, 2, 14, 15, 16, 17, 18, 28, 32 and 44 correspond to H^+, H_2^+, N^+, CH_3^+, CH_4^+, OH^+, H_2O^+, N_2^+, O_2^+, and CO_2^+, respectively [28–32]. Among them, the ion currents at 15, 16 and 44 are related to the carbon composition in plasma. And although it is difficult to identify, we propose that the peaks detected at 91, 107, 121, and 137 might be attributed to $SiO_2CH_3^+$, $SiO_2C_2H_7^+$, $SiO_3C_3H_9^+$ and $SiO_3C_4H_{13}^+$, respectively, on the basis of a possible replacement of methyl or ethyl groups by hydroxyl groups in TMOS [28]. As in the O_2/TEOS case, the ions in the low mass region (mass number up to 44) are created by plasma reaction. When the plasma is switched on, the intensity peaks observed in the mass range of 50–153 amu with the plasma switched off appear with lower relative intensity, which indicates that TMOS and heavy fragments are mostly depleted.

The N_2/TMOS plasma ion currents under the change of N_2 gas flow rate is shown in Fig. 9. The N_2 gas flow rates of 5, 10, 15 sccm are considered with the flow rate of TMOS fixed as 10 sccm. The picture shows that increasing nitrogen gas flow rate results in the increase of the ion currents containing carbon composition [18,28]. Therefore, we suppose that the nitrogen gas flow plays an important role in increasing the carbon composition. Concerning to the consumption of the introduced nitrogen molecules, the production of the CH_4^+ and OH^+ ion in the plasma need a reaction with nitrogen. We observe that as N_2 gas flow rate is increased, the peaks of N and N_2 increase, which is consistent of OES peaks of N in Fig. 6. This tendency is seen up to a certain level of N_2 flow rate (about 20 sccm, which corresponds to $R = 1.11$). On the other hand, as N_2 gas flow rate is increased, the creation of the peaks corresponding TMOS fragments with mass number above 75 is reduced. Instead the peaks corresponding TMOS fragments with mass number between 50 and 75 are increased. This indicates that the increase in the N_2 gas flow promotes the dissociation of the TMOS molecule and the heavy TMOS fragments. This can be accounted for from the observation that N_2 molecules in the plasma have considerable populations in the excited vibrational levels [33]. Through the exothermic near-resonant vibrational–electronic energy-exchange reaction, a larger amount of N_2 gas flow can

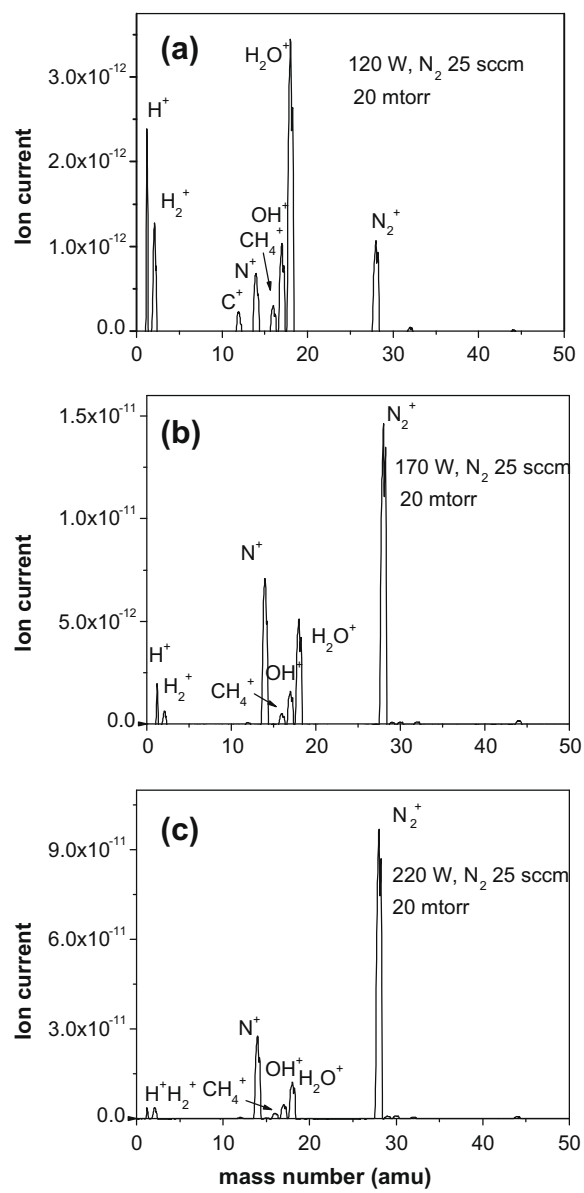

Fig. 10. Mass spectra during discharge at various input power for TMOS and N_2 gas mixture with total pressure of 20 mTorr.

result in more frequent dissociation reaction of the TMOS molecules and the heavy TMOS fragments.

Fig. 10a–c shows typical mass spectra of the neutral species from the discharge obtained at three different input powers, respectively. The most striking effects of increasing the input RF power from 120 to 220 W are the increase in the N^+, N_2^+, CH_4^+, and OH^+ ion relative intensity and the drop of the relative intensity of all the heavy TMOS related peaks. This confirms that the ions in the low mass region (mass number up to 44) are created by the plasma reaction. From comparison of the three mass spectra, it is immediately apparent that an increase in the plasma power promotes the dissociation of the heavy molecules.

4. Conclusion

Thin $SiO_xC_yN_z$ films are deposited from $TMOS/N_2/NH_3$ produced plasmas in an inductively coupled RF reactor. The incorporation of carbon and nitrogen atoms into films of SiO_2 network has been confirmed in the characterizations of the deposited films (ellipsometry, FTIR and XPS) and the plasma phase (OES and mass spectrometry). The composition of the plasma and the composition and structure of the deposited films are studied as a function of the ratio of partial pressure of the TMOS gas to the N_2 gas (R). The FTIR absorption bands from about 850 to 1000 cm^{-1} and 1000 to 1250 cm^{-1}, which can be attributed to the incorporation of nitrogen and carbon atoms, are observed. The optical characteristics of the deposited films are studied by varying the TMOS to N_2 pressure ratio. As the partial pressure of N_2 is decreased, the refractive index begins to decrease, reaches a minimum at $R = 1.71$, and then saturates. We attribute the decrease in the refractive index to the incorporation of more oxygen and carbon atoms. Also, the abundance of nitrogen in the films contributes to the increase in the refractive index. These arguments are examined by XPS and OES data. The XPS results show that the nitrogen content in the films increases with R to the point of $R = 0.7$, then decreases, whereas the oxygen content shows the opposite behavior with varying R. This result is generally in agreement with the discussions of the FTIR results and the refractive index measurements. The emission intensity from O atom in the plasma phase reaches maximum at $R = 1.71$ where the refractive index has the lowest value. The mass spectrometry experiment indicates that the increase in the N_2 gas flow promotes the dissociation of the TMOS molecule and the heavy TMOS fragments and the increase in the plasma power promotes the dissociation of the molecules. A further analysis of the deposition processes and characterization of the thin films is needed to provide an effective control of the composition and microstructure of the films.

Acknowledgment

This work was supported by the research fund of Dong-A University.

References

[1] K.E. Mattsson, J. Appl. Phys. 77 (1995) 6616.
[2] M.N.P. Carreno, M.I. Alayo, I. Pereyra, A.T. Lopes, Sens. Actuator A 100 (2002) 295.
[3] E.C. Samano, J. Camancho, R. Machorro, J. Vac. Sci. Technol. A 23 (2005) 1228.
[4] K. Aumaille, C. Vallee, A. Granier, A. Goullet, F. Gaboriau, G. Turban, Thin Solid Films 359 (2000) 188.
[5] M.S. Kang, T.H. Chung, Y. Kim, Thin Solid Films 506–507 (2006) 45.
[6] C.J. Chung, T.H. Chung, M.S. Kang, Y. Kim, J. Korean Phys. Soc. 49 (2006) 162.
[7] A. Yanguas-Gil, J. Cotrino, A.R. Gonzalez-Elipe, J. Phys. D: Appl. Phys. 40 (2007) 3411.
[8] E.R. Fisher, Plasma Sources Sci. Technol. 11 (2002) A105.
[9] A. Raveh, J. Brewer, E.A. Irene, J. Vac. Sci. Technol. A 19 (2001) 9.
[10] A.M. Wrobel, M.R. Wertheimer, Plasma-polymerized organosilicons and organometallics, in: R. d'Agostino (Ed.), Plasma Treatment and Etching of Polymers, Academic Press, Boston, 1990.
[11] M. Klanisek Gunde, M. Macek, Phys. Status Solidi (a) 183 (2001) 439.
[12] F. Hamelmann, A. Aschentrup, A. Brechling, U. Heinzmann, A. Gushterov, A. Szekeres, S. Simeonov, Vacuum 75 (2004) 307.
[13] A.D. Nara, H. Itoh, Jpn. J. Appl. Phys. 36 (1997) 1477.
[14] D.V. Tsu, G. Lucovsky, M.J. Mantini, S.S. Chao, J. Vac. Sci. Technol. A5 (1987) 1998.
[15] J. Viard, E. Beche, D. Perarnau, R. Berojoan, J. Durand, J. Eur. Ceram. Soc. 17 (1997) 2025.
[16] A. Raveh, J. Brewer, E.A. Irene, J. Vac. Sci. Technol. A19 (2001) 17.
[17] A. Grill, D.A. Neumayer, J. Appl. Phys. 94 (2003) 6697.
[18] M. Modreanu, M. Gartner, N. Tomozeiu, J. Seekamp, P. Cosmin, Opt. Mater. 17 (2001) 145.
[19] T. Roschuk, J. Wojcik, X. Tan, J.A. Davies, P. Mascher, J. Vac. Sci. Technol. A22 (2004) 883.
[20] Y. Inoue, H. Sugimura, O. Takai, Thin Solid Films 386 (2001) 252.
[21] Y. Inoue, O. Takai, Thin Solid Films 316 (1998) 79.
[22] M. Kannan, C.S. Yang, C.K. Choi, J. Korean Phys. Soc. 45 (2004) S944.
[23] G.J. Wan, P. Yang, R.K.Y. Fu, Z.Q. Yao, N. Huang, Paul K.J. Chu, Vac. Sci. Technol. A23 (2005) 1346.
[24] A. Dasgupta, C.G. Takoudis, Thin Solid Films 436 (2003) 162.
[25] H. Ono, T. Ikarashi, Y. Miura, E. Hasegawa, K. Ando, T. Kitano, Appl. Phys. Lett. 74 (1999) 203.
[26] S.B. Bang, T.H. Chung, Y. Kim, Thin Solid Films 444 (2003) 125.
[27] K. Aumaille, A. Granier, M. Schmidt, B. Grolleau, C. Vallee, G. Tuban, Plasma Sources Sci. Technol. 9 (2000) 331.
[28] Y. Inoue, O. Takai, Thin Solid Films 341 (1999) 419.
[29] N.M. Horii, K. Okimura, A. Shibata, Thin Solis Films 343–344 (1999) 148.
[30] F. Fracassi, R. d'Aostino, P. Favia, J. Electrochem. Soc. 139 (1992) 2636.
[31] Y. Inoue, H. Sugimura, O. Takai, Thin Solid Films 345 (2001) 90.
[32] Y. Inoue, O. Takai, Plasma Sources Sci. Technol. 5 (1996) 339.
[33] P.A. Sa, J. Loureiro, J. Phys. D: Appl. Phys. 30 (1997) 2320.